

ACCEPTED MANUSCRIPT

This is an early electronic version of an as-received manuscript that has been accepted for publication in the Journal of the Serbian Chemical Society but has not yet been subjected to the editing process and publishing procedure applied by the JSCS Editorial Office.

Please cite this article as F. Motaghi and H. Mohammadi-Manesh, *J. Serb. Chem. Soc.* (2025) <https://doi.org/10.2298/JSC240810011M>

This “raw” version of the manuscript is being provided to the authors and readers for their technical service. It must be stressed that the manuscript still has to be subjected to copyediting, typesetting, English grammar and syntax corrections, professional editing and authors’ review of the galley proof before it is published in its final form. Please note that during these publishing processes, many errors may emerge which could affect the final content of the manuscript and all legal disclaimers applied according to the policies of the Journal.



J. Serb. Chem. Soc. **00(0)** 1-14 (2024)
JSCS-13006

Enhancing hydrogen evolution reaction using transition metal atoms on 6,6,12-graphyne: A DFT study

FATEMEH MOTAGHI AND HOSSEIN MOHAMMADI-MANESH*

Department of Chemistry, Faculty of Science, Yazd University, Yazd, Iran.

(Received 10 August 2024; revised 17 November 2024; accepted 27 January 2025)

Abstract: The escalating global population and the urgent need for sustainable energy solutions with minimal environmental impact have underscored the significance of developing renewable energy sources. Hydrogen, as an energy carrier and fuel, presents substantial advantages over other energy forms, alongside diverse applications in medical treatments and the production of critical chemicals like methane and methanol. Thus, hydrogen emerges as a potential alternative to fossil fuel, offering a stable and clean energy solution. In this study, we present a theoretical design of transition metal (TM) anchored 6,6,12-graphyne (GY) based catalysts for the hydrogen evolution reaction (HER) using density functional theory (DFT). Our findings reveal that among all evaluated systems, cobalt single-atom catalyst (SAC) anchored on 6,6,12-graphyne exhibit the highest thermodynamic stability and superior HER catalytic performance, with a remarkably low ΔG_{H^*} value of 0.042 eV. We have investigated the density of states, HOMOs, LUMOs, electron density, and band structures of our designed SACs. This work provides a practical strategy for experimental groups to effectively tune the electronic structures of catalysts and enhance their catalytic activity.

Keywords: single-atom catalysts; density functional theory; HER.

INTRODUCTION

The global population has surpassed seven billion and is projected to exceed nine billion by the mid-21st century.¹ Correspondingly, energy consumption is anticipated to rise from 16 terawatts (TW) in 2010 to 23 TW by 2030 and potentially 30 TW by 2050.² The critical challenges posed by environmental issues and the extensive consumption of fossil fuels necessitate the development of high-efficiency, green, and sustainable energy technologies.³ Consequently, the demand for renewable energy sources has surged, as conventional non-renewable energy sources are finite. Renewable energy sources such as solar, wind, and thermal

* Corresponding author. E-mail: mohammadimanesh@yazd.ac.ir
<https://doi.org/10.2298/JSC240810011M>

energy offer alternatives to traditional fossil fuels.⁴ However, the uneven distribution of these energy sources limits their large-scale applications.

Hydrogen is a clean and versatile energy carrier with significant potential as a sustainable alternative to fossil fuels in future energy systems.⁵ Molecular hydrogen gas (H₂) is particularly attractive due to its high gravimetric energy density (the amount of energy released per kilogram of fuel) and its environmentally friendly combustion, which produces only water. This makes hydrogen an ideal candidate for low-carbon energy applications.⁶

Currently, most H₂ is produced via steam reforming of fossil fuels. However, it can also be generated from renewable sources such as water and biomass, as well as non-renewable sources like hydrogen sulfide. Water, one of the most abundant resources on Earth, is a primary candidate for hydrogen production through water-splitting methods.^{1,7}

Hydrogen can be stored in various materials, including metal organic frameworks, owing to their high surface area, customizable structures, and versatile applications.⁸

The fundamental reactions in water splitting include the hydrogen evolution reaction (HER) and the oxygen evolution reaction (OER). The production and storage of hydrogen via electrochemical water splitting have garnered significant attention from scientific communities, industries, and governments worldwide. Under suitable conditions, water molecules can be decomposed into hydrogen and oxygen through various methods and energy inputs, including electrolysis powered by renewable energy sources.

One major challenge in this field is the design of electrocatalysts for HER that offer appropriate efficiency at a reasonable cost. Precious metals and their oxides have traditionally been used as water-splitting catalysts, but their high costs and scarcity hinder widespread commercialization.⁹ To overcome the high energy barrier of HER, an efficient catalyst is required.¹⁰ Single-atom catalysts (SACs) are gaining increasing attention due to their unique properties, including maximum atom utilization efficiency, low cost, high activity, and high selectivity.^{11–15}

A novel class of 2D graphyne nanosheets, featuring suitable porous carbon structures with sp-hybridized carbon atoms, has been synthesized and proven effective for supporting single atoms.^{16–18} Graphdiyne, an allotrope of graphyne, has demonstrated promise as a nanomaterial for electrolysis^{12,19,20} and was synthesized by Lee's group.²¹ One type of graphyne, GY, exhibits remarkable properties that have led to various applications and considerable research interest. Numerous studies have sought cost-effective electrocatalysts based on non-precious transition metals, including Mo, Co, Ni, Fe, and their complexes.^{22,23}

Tianwei *et al.* decorated graphdiyne with first-row transition metals (from Sc to Zn) and Pt, investigating their efficacy as electrocatalysts for water splitting. Their results showed that graphdiyne decorated with scandium, titanium,

vanadium, iron, and platinum exhibited high catalytic activity towards HER. Additionally, calculations indicated that graphdiyne decorated with platinum and nickel are promising bifunctional electrocatalysts for water splitting.¹² Faizan *et al.* used density functional theory to design and investigate first-row transition metal monoatomic catalysts supported on graphyne, concluding that Ni SAC supported on graphyne showed the highest thermodynamic stability and best HER catalytic performance with a ΔG_{H^*} value of 0.08 eV.²⁴ Uwamungu *et al.* studied the stability and electronic properties of iron-doped graphyne-like BN-yne nanosheets, finding that HER is significantly influenced by charge redistribution caused by iron on the surface, increasing the number of active sites. Thus, iron-doped graphyne-like BN-yne can be considered a promising electrocatalyst for HER.²³

Among the different types of graphyne structures, 6,6,12-graphyne stands out due to its significant thermal conductivity and directional anisotropy, attributed to its non-sixfold symmetric structure. Despite the promising characteristics of graphynes as electrocatalysts for water splitting reactions, 6,6,12-graphyne (GY) has not yet been explored as an electrocatalyst for the hydrogen evolution reaction (HER). This research aims to fill this gap by employing density functional theory (DFT) computations to investigate the potential of GY, with single transition metal atoms (TM = Fe, Co, Ni, Cu) anchored on its structure, to enhance HER catalytic activities. This study highlights the novelty of utilizing GY for HER, showcasing its unique properties and significant potential as a high-performance electrocatalyst.

COMPUTATIONAL METHOD

In this research, all calculations were performed using density functional theory (DFT) via the Dmol3 code (version 17.1.0.48).²⁵ The generalized gradient approximation (GGA) with the Perdew-Burke-Ernzerhof (PBE) functional was employed to describe exchange-correlation interactions.²⁶ The numerical double-numerical plus polarization (DNP) basis set, comparable in quality to 6-31G sets, was used for all atoms. The long-range van der Waals interactions were described using the empirical correction in Grimme's scheme.²⁷ A convergence threshold of 10^{-6} Hartree for electronic self-consistent field (SCF) calculations and 10^{-5} Hartree for total energy, 0.002 Hartree/Å for maximum force, and 0.005 Å for maximum displacement for geometry optimization were adopted. A $7 \times 7 \times 1$ Monkhorst-Pack k-mesh was used for sampling the Brillouin zone during the structural optimization of the supercell (2×2 unit cell) and for electronic structure calculations. To simulate the H₂O solvent environment with a dielectric constant of 78.54, a conductor-like screening model (COSMO) was employed in all calculations.²⁸

The intermediate states in HER (H*) were investigated by exploring multiple initial configurations for hydrogen adsorption on both GY and TM@GY electrocatalysts. The subsequent analysis focused on the most energetically favorable adsorption structures, determined based on their minimum adsorption energies (ΔE_{ads}). These ΔE_{ads} values were calculated using the following equation²⁹:

$$\Delta E_{ads} = E_{\text{substrate} + \text{adsorbent}} - E_{\text{substrate}} - E_{\text{adsorbent}} \quad (1)$$

where $E_{\text{adsorbent}}$, $E_{\text{substrate}}$, and $E_{\text{substrate} + \text{adsorbent}}$ are the total energies of the adsorbent, the substrate, and the substrate-adsorbent composites, respectively. More negative ΔE_{ads} values indicate stronger binding between the catalyst and the intermediate, as well as better thermodynamic stability.

Hydrogen production from water splitting involves two steps: a) atomic H adsorption on the catalysts, and b) formation and release of H_2 molecules.³⁰ When one H atom is adsorbed on the catalyst, the calculated intermediate state energy determines the HER reaction barrier (overpotential for the electron). Consequently, HER performance can be assessed through ΔG_{H^*} . The following equation describes the production of H_2 ³¹:



where * and H^* represent the active site and the adsorbed intermediate, respectively. Under standard conditions ($\text{pH} = 0$, $U = 0$, and 298.15 K), the chemical potential of $\text{H}^+ + e^-$ ($\mu_{(\text{H}^+ + e^-)}$) is equivalent to that of $1/2 \text{H}_2$ ($1/2 \mu_{\text{H}_2}$). In other words, $\mu_{(\text{H}^+ + e^-)} = 1/2 \mu_{\text{H}_2}$, based on the calculation hydrogen electrode model.³¹ The ideal ΔG_{H^*} value for HER is zero. Both weak and strong binding energy of the intermediate state can lead to poor HER efficiency. Therefore, ΔG_{H^*} is obtained by the following equation²⁹:

$$\Delta G_{\text{H}^*} = \Delta E_{\text{H}^*} + \Delta E_{\text{ZPE}} - T\Delta S_{\text{H}^*} \quad (3)$$

where ΔE_{H^*} is the energy of hydrogen adsorption, obtained from equation (1). ΔS_{H^*} is the entropy difference between the gas phase and the adsorbed state, and T is the temperature at 298 K. ΔE_{ZPE} is the zero-point energy difference between the H_2 gas phase and the adsorbed H, given by³²:

$$\Delta E_{\text{ZPE}} = E_{\text{ZPE}}^{\text{H}^*} - E_{\text{ZPE}}^* - \frac{1}{2} E_{\text{ZPE}}^{\text{H}_2} \quad (4)$$

where E_{ZPE}^* is the zero-point energy of the pristine substrate, $E_{\text{ZPE}}^{\text{H}^*}$ is the zero-point energy of adsorbed hydrogen on the substrate, and $E_{\text{ZPE}}^{\text{H}_2}$ is the zero-point energy of gas-phase H_2 . Due to the small calculated vibrational entropy of the adsorbed state H^* , the adsorption entropy of $1/2 \text{H}_2$ is $\Delta S_{\text{H}} \approx -0.5 S_{\text{H}_2}^0$, where $S_{\text{H}_2}^0$ is the entropy of gas-phase H_2 , approximately 130 J/(mol·K) under standard conditions.³³ According to Nørskov's hypothesis,²⁸ the overpotential of the hydrogen evolution reaction (η^{HER}) is obtained using the following equation:

$$\eta^{\text{HER}} = \frac{|\Delta G_{\text{H}^*}|}{e} \quad (5)$$

To explain the HER kinetics under standard conditions, $|\Delta G_{\text{H}^*}|$ is used to derive the volcano curve for the theoretical exchange current (i_0)³⁴:

$$i_0 = -ek_0 \frac{1}{1 + \exp(|\Delta G_{\text{H}^*}|/k_b T)} \quad (6)$$

where k_b , k_0 and T are the Boltzmann constant, the reaction rate constant at zero overpotential, and the temperature, respectively. For illustrative purposes, k_0 is set to 1. Additionally, molecular dynamics (MD) simulations with an NVT ensemble were used to evaluate the thermodynamic stability of the catalysts. The MD simulation lasted for 2000 steps with a time step of 2.0 fs, and the temperature was controlled at 300 K using the Nosé–Hoover chains method.³⁵

RESULTS AND DISCUSSION

HER performance of pure GY

In this section, we present our findings on the performance of GY-based TM as a HER catalyst. We began our investigation by examining the GY monolayer (Fig. 1). To ensure accurate results, we used a supercell large enough to prevent interactions between adsorbates in two periodic units. Figure 2 illustrates the density of states (DOS) and the band structure of the supercell. Our calculations revealed that the band gap of 6,6,12-graphyne is 0.061 eV. Following this initial characterization, we proceeded to evaluate the HER performance of various TM atoms anchored on the GY structure. Our aim was to identify promising electrocatalysts for the HER based on their performance at different active sites.

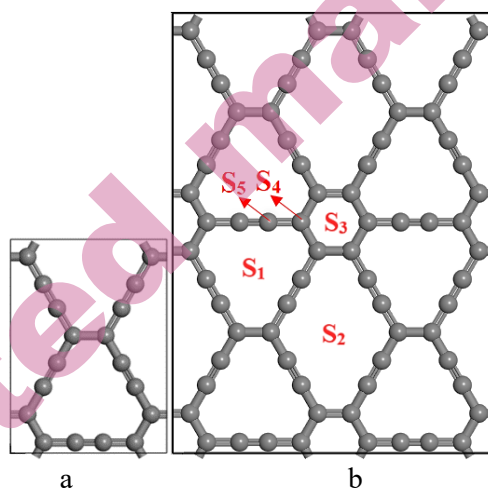


Fig. 1. (a) The GY unit cell; (b) The (2×2) GY supercell, showing the possible binding sites (S_1 , S_2 , S_3 , S_4 and S_5) for single TM atoms and the hydrogen intermediate.

We further decorated GY with various TMs (TM = Fe, Co, Ni, Cu) at the five introduced sites. The binding energies were negative for all structures. According to the results, when the metal atom is anchored at S_1 , the binding energies are much larger than at other sites, indicating that S_1 is the most energetically stable site. The binding energies for Fe@GY, Co@GY, Ni@GY, and Cu@GY were -5.76, -5.72, -5.92, and -3.76 eV, respectively. Additionally, the most negative absorption energy is related to nickel. These large binding energies indicate strong chemisorption between the GY monolayer and TM atoms, which is favorable for catalytic processes.

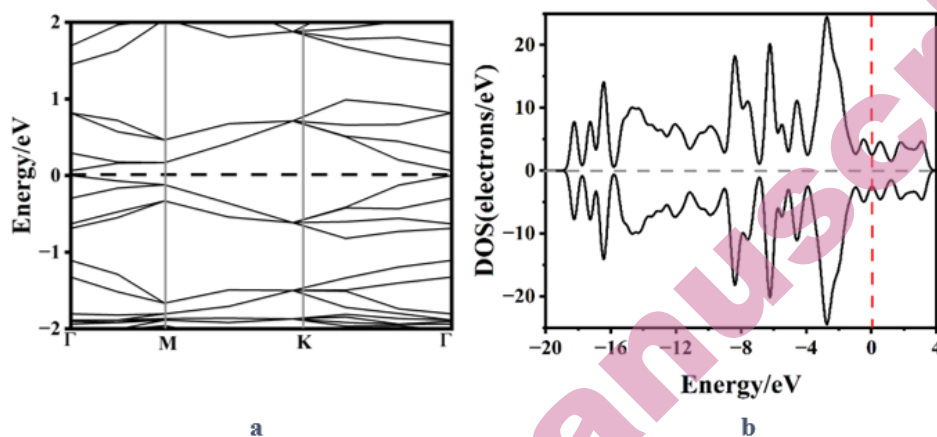


Fig. 2. (a) The band structures of the 2×2 supercell GY; (b) DOS of the 2×2 supercell GY, with the Fermi level indicated by the red dashed line.

To evaluate pure GY as an electrocatalyst for hydrogen production, the adsorption of intermediate H at five different sites with varying distances on the GY substrate was investigated. The results are listed in Table I. According to Table I, the energy of hydrogen adsorption at the S_5 site (sp-hybridized C) is thermodynamically favorable, with a Gibbs free energy change and overpotential of 0.15 eV and 0.15 V, respectively.

Table I. Final distance of H intermediate from the substrate, total energy (E_{total}) and absorption energy (E_{ad}) at different sites

Site	Distance / Å	E_{total} / eV	E_{ad} / eV
S_1	1.10	-74582.70	0.15
S_2	2.02	-74580.63	2.22
S_3	2.23	-74579.90	2.95
S_4	1.10	-74582.51	0.35
S_5	1.10	-74582.83	0.02

The formation energies of TM@GY were further calculated using the expression $E_f = E_{\text{total}} + \mu_C - (E_{\text{GY}} + E_{\text{TM}})$, where E_{total} is the total energy of TM@GY, E_{GY} is the energy of pristine GY, E_{TM} is the energy per atom of the transition metal, and μ_C is the chemical potential of a single C atom in GY. The formation energies for Co@GY, Ni@GY, Fe@GY, and Cu@GY were -5.72, -5.93, -5.76, and -3.76 eV, respectively. These low formation energies suggest that TM@GY catalysts can be easily synthesized experimentally.³⁶ The thermodynamic stability of the Co@GY catalyst was tested under standard conditions. The results indicated that the energies oscillate near the equilibrium state, with no significant structural reconstruction at the end of the MD simulation

(Fig. 3), demonstrating the good thermodynamic stability of Co@GY in the HER catalytic process.

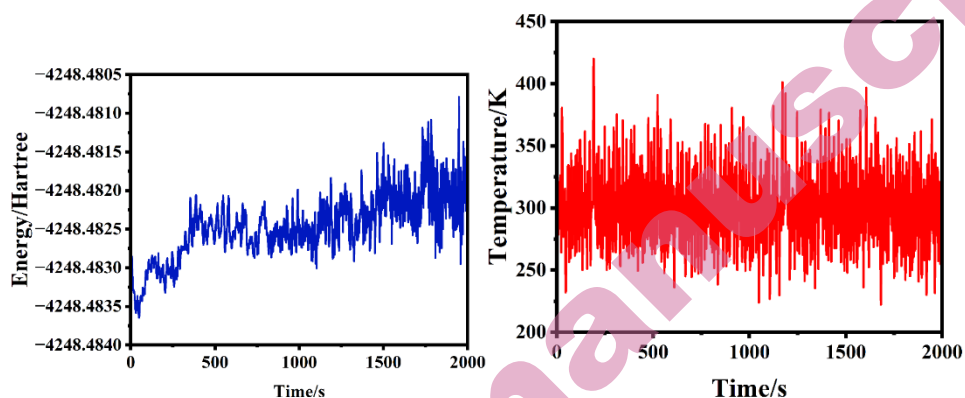


Fig. 3. Fluctuations of energy and temperature during MD simulations of Co@GY catalyst.

Stability, and electronic properties of structures

The band structures of Fe@GY, Co@GY, Ni@GY, and Cu@GY were computed to assess their electrical conductivities. As shown in Fig. 4, there is no effect of spin polarization for Co@GY, Ni@GY, and Cu@GY, with no difference between the states related to alpha and beta spins, indicating no magnetic moment creation. For Fe@GY, the alpha and beta spins do not align, creating a local magnetic moment. The energy gap for Ni@GY is 0.024 eV, while it is zero for the other structures. HOMOs and LUMOs are shown in Fig. S1.

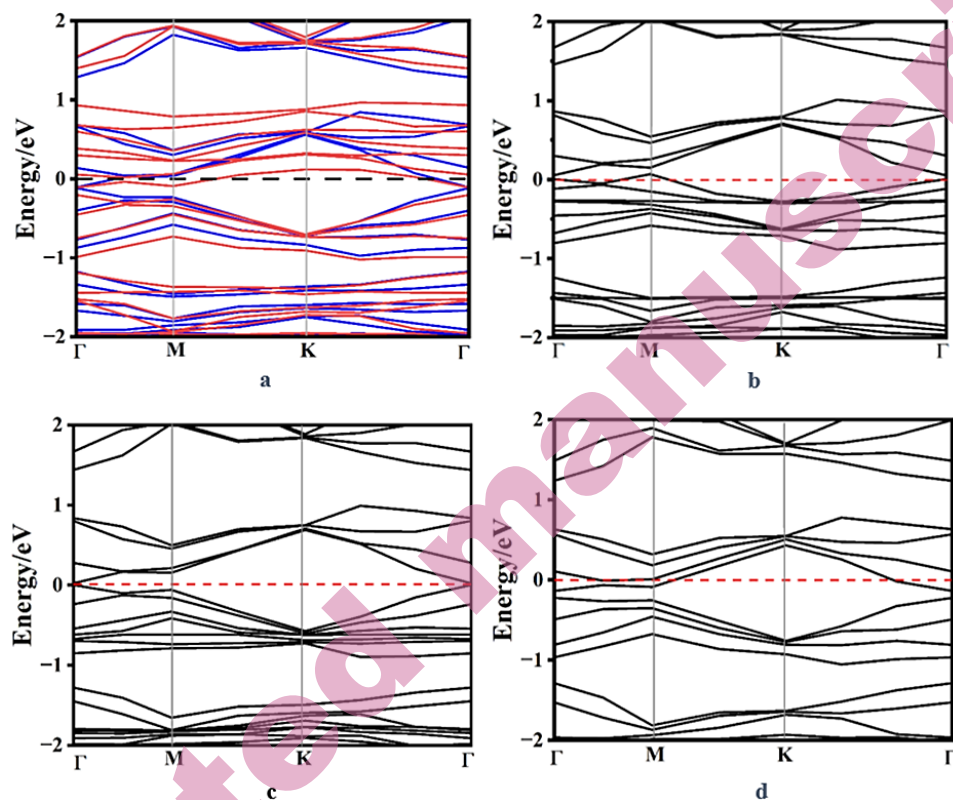


Fig. 4. Band structures (at GGA-PBE level) of (a) Fe@GY, (b) Co@GY, (c) Ni@GY, and (d) Cu@GY, with the zero line indicating the Fermi level.

The density of states (DOS) in Fig. 2 shows the semimetallic property of the pristine GY monolayer. Importantly, all TM@GY nanosheets present decreased band gaps and most exhibit metallic properties after decorating with TM atoms. The PDOS for TM@GY is presented in Fig. 5. The predominant peaks of TM-d states crossing the Fermi level imply high carrier density, enhancing electronic conductivity of TM@GY monolayers and favoring electrocatalytic processes. The difference electron density of TM@GY are also calculated (Fig. 6), showing Co@GY and Ni@GY catalysts display more charge density, especially over the acetylenic ring.

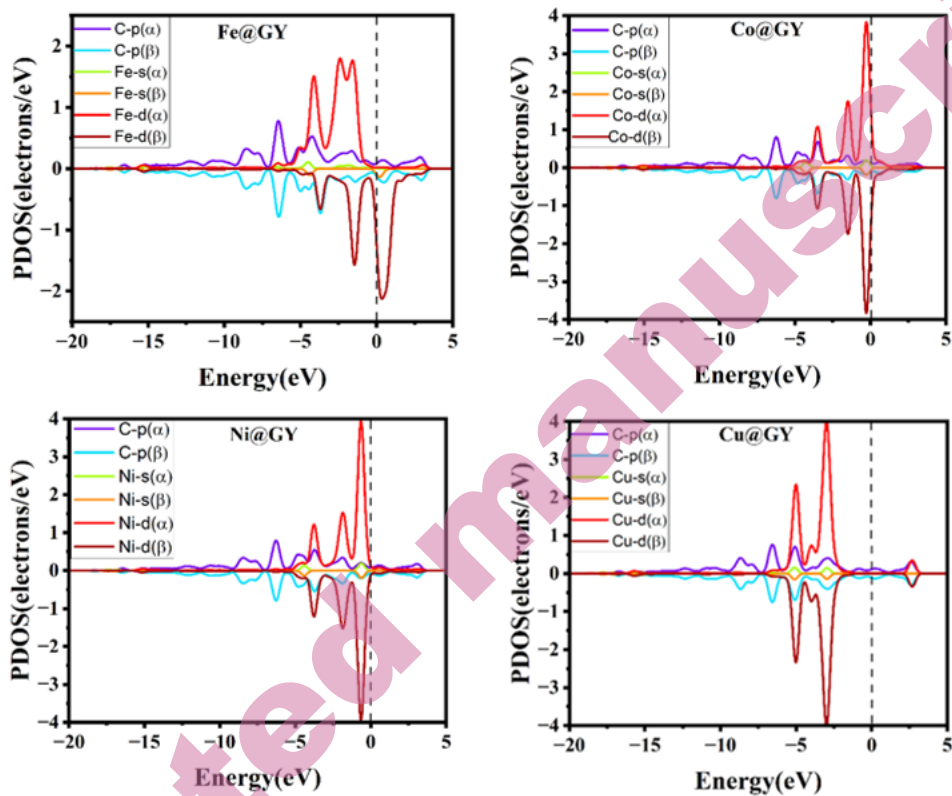


Fig. 5. Partial density of states (PDOS) of TM@GY. The Fermi level is set to zero.

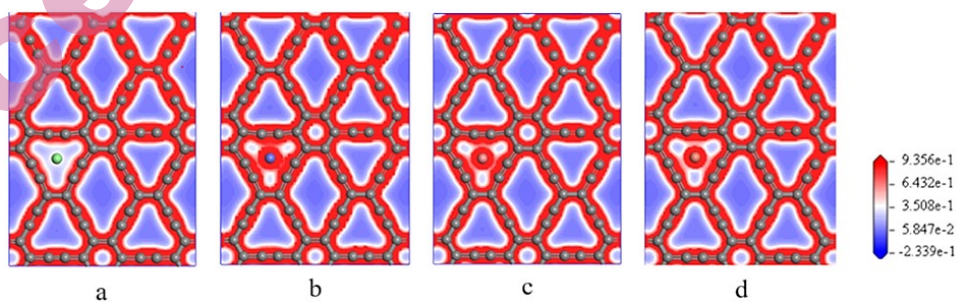


Fig. 6. Difference electron density images of (a) Fe@GY, (b) Co@GY, (c) Ni@GY, and (d) Cu@GY; blue and red colors represent charge depletion and accumulation, respectively.

HER performance of TM@GY

The origin of the electrocatalytic activity of TM@GY catalysts for HER is explored. Table II presents the ΔG_{H^*} values for H* adsorption on pristine GY and on 6,6,12 - graphyne decorated with various TMs. For the S₅ site of pristine GY, the ΔG_{H^*} value is 0.15 eV, indicating a weak binding strength between C and H atoms. However, after decorating the GY monolayer with TM atoms, the acetylenic C and sp and sp² hybridized carbon atoms of TM@GY samples can become active sites (Fig. 7). This modification significantly alters the hydrogen adsorption properties of the material, potentially enhancing its catalytic activity for HER.

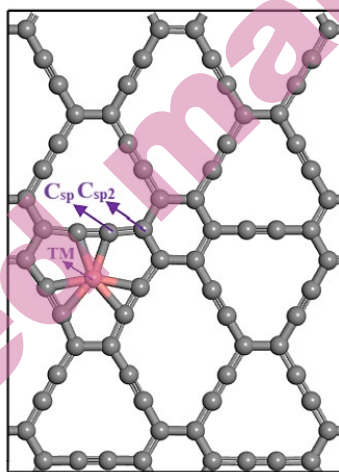


Fig. 7. Possible active sites on TM@GY for the hydrogen evolution reaction.

The TM@GY catalyst shows an increased number of active sites and enhanced catalytic performance, particularly at the Co, Fe (C_{sp}), and Co (C_{sp}) sites, with ΔG_{H^*} values of 0.042, 0.044, and 0.060 eV, respectively. These values are comparable to the state-of-the-art Pt catalysts (-0.09 eV)³⁷ and close to the ideal value ($\Delta G_{H^*} = 0$ eV), indicating that decorating TM atoms at the acetylenic ring is an effective strategy for increasing active sites and boosting catalytic activity for HER. The electron transfer from TM atoms to acetylenic carbon atoms improves the interaction between H and acetylenic C atoms (Table S1), moving ΔG_{H^*} closer to zero. These changes are attributed to charge redistribution introduced by TM atom decoration.³⁸ According to Table II, Ni@GY and Cu@GY are unsuitable catalysts for hydrogen production, as all values are positive. The most stable adsorption configurations are shown in Fig. S2.

Table II. Calculated Gibbs free energy changes (eV) of the H atom binding on GY and TM (ΔG_H (TM)) and carbon atoms (ΔG_H (C_{sp}) and (ΔG_H (C_{sp2})) for different TMs supported on GY

TM@GY	$\Delta G_{\text{H}}(\text{TM})$	$\Delta G_{\text{H}}(\text{C}_{\text{sp}2})$	$\Delta G_{\text{H}}(\text{C}_{\text{sp}})$
Fe@GY	0.453	0.601	0.044
Co@GY	0.042	0.624	0.060
Ni@GY	0.954	0.189	0.590
Cu@GY	1.810	0.178	0.501
GY	-	-	0.15

The volcano diagram in Figure 8 reveals that the data points for the cobalt and sp carbon sites in Co@GY, as well as the sp carbon in Fe@GY, are positioned very close to the volcano peak. This proximity indicates that the Gibbs free energy (ΔG_{H^*}) for the adsorption of intermediate hydrogen species at these sites is nearly zero, representing an optimal balance between hydrogen adsorption and desorption processes. Such favorable energetic conditions lead to a decreased overpotential, minimizing the energy barrier for hydrogen adsorption and desorption steps, while also enhancing the efficiency of the hydrogen evolution reaction (HER). Consequently, these sites exhibit improved catalytic activity compared to other positions on the catalyst surface, suggesting that Co@GY and Fe@GY, particularly at their sp carbon sites, could be promising candidates for highly efficient HER electrocatalysts.

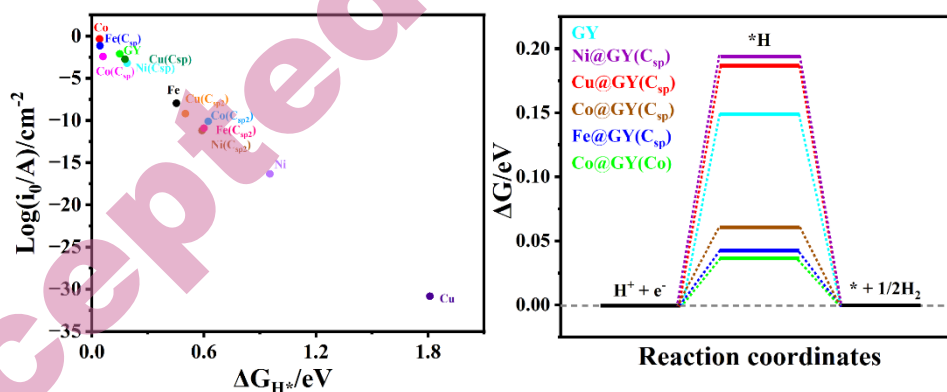


Fig. 8. Hydrogen evolution reaction volcano curve of exchange current (i_0) plotted as a function of the Gibbs free energy of H^* (ΔG_{H^*}) adsorption on possible active sites of GY and TM@GY catalysts and Calculated free energy diagram for TM@GY catalysts under standard conditions (pH = 0, U = 0 relative to the standard hydrogen electrode, and 298.15 K).

CONCLUSION

In this study, we computationally screened four single TM atoms decorated on GY as potential catalysts for HER. The calculated results demonstrate that single TM atoms can strongly bind at the acetylenic-ring center of the GY monolayer, exhibiting metallic properties or reduced band gaps. The strong binding strength of these single TM atoms indicates that the GY monolayer is an

excellent substrate for designing SACs. Among the catalysts studied, Co@GY exhibited the best HER performance with a minimum ΔG_{H^*} of 0.042 eV, closely followed by Fe@GY with a ΔG_{H^*} of 0.044 eV at the sp-hybridized carbon atom site. These findings provide valuable insights for designing new, high-performance electrocatalysts for HER. Our results underscore the potential of GY decorated with single non-precious metals as promising alternative HER catalysts, offering a path towards more efficient and cost-effective hydrogen production technologies.

SUPPLEMENTARY MATERIAL

Additional data are available electronically at the pages of journal website: <https://www.shd-pub.org.rs/index.php/JSCS/article/view/13006>, or from the corresponding author on request.

ИЗВОД

ПОБОЉШАЊЕ РЕАКЦИЈЕ ИЗДВАЈАЊА ВОДОНИКА КОРИШЋЕЊЕМ АТОМА МЕТАЛА НА 6,6,12-ГРАФИНУ: DFT СТУДИЈА

FATEMEH MOTAGHI, HOSSEIN MOHAMMADI-MANESH¹*Department of Chemistry, Faculty of Science, Yazd University, Yazd, Iran.*

Нагли раст глобалног становништва и хитна потреба за одрживим решењима за енергијом са минималним утицајем на животну околину, истакали су значај развијања обновљивих извора енергије. Водоник, као носилац енергије и гориво, представља битну предност над другим облицима енергије, поред осталог има примену у медицинским поступцима и производњи критичних хемикалија, попут метана и метанола. Тако се водоник јавља као потенцијална алтернатива фосилним горивима, нудећи стабилно и чисто решење за енергију. У овој студији представљамо теоријски дизајн катализатора заснованог на прелазном металу (ТМ) закаченом на 6,6,12-графин (GY) за реакцију издвајања водоника (HER) користећи теорију функционала густине (DFT). Наши налази откривају да од свих испробаних система, кобалтов једноатомски катализатор (SAC) закачен за 6,6,12-графин испољава највишу термодинамичку стабилност, испољавајући највишу термодинамичку стабилност и надмоћно HER каталитичко дејство, са уочљиво ниском вредношћу ΔG_{H^*} од 0,042 eV. Испитивали смо густину стања, HOMO, LUMO, електронску густину и структуру трака наших дизајнираних SAC-ова. Овај рад обезбеђује практичну стратегију за експериментаторске групе да ефикасно подесе електронске структуре катализатора и повећају њихову каталитичку активност.

(Примљено 10. августа 2024; ревидирано 17. новембра 2024; прихваћено 27. јануара 2025.)

REFERENCES

1. F. Safari, I. Dincer, *Energy Convers. Manag.* **205** (2020) 112182 (<https://doi.org/10.1016/j.enconman.2019.112182>)
2. N. S. Lewis, D. G. Nocera, *Proc. Natl. Acad. Sci.* **103** (2006) 15729–15735 (<https://doi.org/10.1073/pnas.0603395103>)

3. S. Chu, A. Majumdar, *Nature* **488** (2012) 294–303 (<https://doi.org/10.1038/nature11475>)
4. A. Rahman, O. Farrok, M. M. Haque, *Renew. Sustain. Energy Rev.* **161** (2022) 112279 (<https://doi.org/10.1016/j.rser.2022.112279>)
5. J. A. Turner, *Science* **305** (2004) 972–974 (<https://doi.org/10.1126/science.1103197>)
6. C. Energy, *ANational Vision of America's Transition to a Hydrogen Economy - to 2030 and Beyond*. in *Natl. Hydrog. Vis. Meet. Washingt. DC, Novemb., 2002*, pp. 15–16 (<https://doi.org/10.3390/sul3042214>)
7. M. Genovese, A. Schlüter, E. Scionti, F. Piraino, O. Corigliano, P. Fragiaco, *Int. J. Hydrogen Energy* **48** (2023) 16545–16568 (<https://doi.org/10.1016/j.ijhydene.2023.01.194>)
8. Y. H. Hu, L. Zhang, *Adv. Mater.* **22** (2010) E117–E130 (<https://doi.org/10.1002/adma.200902096>)
9. Y. Lee, J. Suntivich, K. J. May, E. E. Perry, Y. Shao-Horn, *J. Phys. Chem. Lett.* **3** (2012) 399–404 (<https://doi.org/10.1021/jz2016507>)
10. Y. Yang, J. Liu, F. Liu, Z. Wang, D. Wu, *J. Mater. Chem. A* **9** (2021) 2438–2447 (<https://doi.org/10.1039/D0TA09903A>)
11. T. Matthews, T. A. Mashola, K. A. Adegoke, K. Mugadza, C. T. Fakude, O. R. Adegoke, A. S. Adekunle, P. Ndungu, N. W. Maxakato, *Coord. Chem. Rev.* **467** (2022) 214600 (<https://doi.org/10.1016/j.ccr.2022.214600>)
12. T. He, S. K. Matta, G. Will, A. Du, *Small Methods* **3** (2019) 1800419 (<https://doi.org/10.1002/smtd.201800419>)
13. L. Gao, F. Wang, M. Yu, F. Wei, J. Qi, S. Lin, D. Xie, *J. Mater. Chem. A* **7** (2019) 19838–19845 (<https://doi.org/10.1039/C9TA06470B>)
14. Y. Feng, L. Zhou, Q. Wan, S. Lin, H. Guo, *Chem. Sci.* **9** (2018) 5890–5896 (<https://doi.org/10.1039/C8SC00776D>)
15. Y. Chen, S. Ji, C. Chen, Q. Peng, D. Wang, Y. Li, *Joule* **2** (2018) 1242–1264 (<https://doi.org/10.1016/j.joule.2018.06.019>)
16. Y. Li, L. Xu, H. Liu, Y. Li, *Chem. Soc. Rev.* **43** (2014) 2572–2586 (<https://doi.org/10.1039/C3CS60388A>)
17. Q. Li, C. Yang, L. Wu, H. Wang, X. Cui, *J. Mater. Chem. A* **7** (2019) 5981–5990 (<https://doi.org/10.1039/C8TA10317H>)
18. C. Huang, Y. Li, N. Wang, Y. Xue, Z. Zuo, H. Liu, Y. Li, *Chem. Rev.* **118** (2018) 7744–7803 (<https://doi.org/10.1039/C3CS60388A>)
19. X. Yin, H. Wang, S. Tang, X. Lu, M. Shu, R. Si, T. Lu, *Angew. Chemie Int. Ed.* **57** (2018) 9382–9386 (<https://doi.org/10.1002/anie.201804817>)
20. Y. Qian, P. Du, P. Wu, C. Cai, D. F. Gervasio, *J. Phys. Chem. C* **120** (2016) 9884–9896 (<https://doi.org/10.1021/acs.jpcc.6b02670>)
21. G. Li, Y. Li, H. Liu, Y. Guo, Y. Li, D. Zhu, *Chem. Commun.* **46** (2010) 3256–3258 (<https://doi.org/10.1039/B922733D>)
22. Y. Yang, Y. Liang, M. Guo, T. Yu, K. Xu, L. Lu, C. Yuan, *Int. J. Hydrogen Energy* **46** (2021) 50–60 (<https://doi.org/10.1016/j.ijhydene.2020.10.194>)
23. Y. Sun, T. Zhang, C. Li, K. Xu, Y. Li, *J. Mater. Chem. A* **8** (2020) 13415–13436 (<https://doi.org/10.1039/D0TA05038E>)
24. F. Ullah, K. Ayub, T. Mahmood, *Int. J. Hydrogen Energy* **46** (2021) 37814–37823 (<https://doi.org/10.1016/j.ijhydene.2021.09.063>)
25. B. Delley, *J. Chem. Phys.* **113** (2000) 7756–7764 (<https://doi.org/10.1063/1.1316015>)

26. J. P. Perdew, J. A. Chevary, S. H. Vosko, K. A. Jackson, M. R. Pederson, D. J. Singh, C. Fiolhais, *Phys. Rev. B* **46** (1992) 6671 (<https://doi.org/10.1103/PhysRevB.46.6671>)
27. S. Grimme, *J. Comput. Chem.* **27** (2006) 1787–1799 (<https://doi.org/10.1002/jcc.20495>)
28. A. Klamt, G. Schüürmann, *J. Chem. Soc. Perkin Trans. 2* (1993) 799–805 (<https://doi.org/10.1039/P29930000799>)
29. A. Kumar, M. I. Sayyed, O. P. Doshi, T. J. Al-Musawi, A. Makrariya, A. A. Lagum, H. Saraireh, M. M. Kadhim, *Mater. Chem. Phys.* **305** (2023) 127892 (<https://doi.org/10.1016/j.matchemphys.2023.127892>)
30. J. K. Nørskov, T. Bligaard, A. Logadottir, J. R. Kitchin, J. G. Chen, S. Pandalov, U. Stimming, *J. Electrochem. Soc.* **152** (2005) J23 (<http://dx.doi.org/10.1149/1.1856988>)
31. J. K. Nørskov, J. Rossmeisl, A. Logadottir, L. Lindqvist, J. R. Kitchin, T. Bligaard, H. Jonsson, *J. Phys. Chem. B* **108** (2004) 17886–17892 (<https://doi.org/10.1021/jp047349j>)
32. X. Gao, Y. Zhou, Z. Cheng, Y. Tan, S. Liu, Z. Shen, *Int. J. Hydrogen Energy* **44** (2019) 27421–27428 (<https://doi.org/10.1016/j.ijhydene.2019.08.195>)
33. Q. Tang, D. Jiang, *Acs Catal.* **6** (2016) 4953–4961 (<https://doi.org/10.1021/acscatal.6b01211>)
34. X. Gao, Y. Zhou, Y. Tan, S. Liu, Z. Cheng, Z. Shen, *Appl. Surf. Sci.* **492** (2019) 8–15 (<https://doi.org/10.1016/j.apsusc.2024.100073>)
35. G. J. Martyna, M. L. Klein, M. Tuckerman, *J. Chem. Phys.* **97** (1992) 2635–2643 (<https://doi.org/10.1063/1.463940>)
36. X. Gao, Y. Zhou, S. Liu, Z. Cheng, Y. Tan, Z. Shen, *Appl. Surf. Sci.* **502** (2020) 144155 (<https://doi.org/10.1016/j.apsusc.2019.144155>)
37. Y.-J. Wang, N. Zhao, B. Fang, H. Li, X. T. Bi, H. Wang, *Chem. Rev.* **115** (2015) 3433–3467 (<https://doi.org/10.1021/cr500519c>)
38. T. He, G. Gao, L. Kou, G. Will, A. Du, *J. Catal.* **354** (2017) 231–235 (<https://doi.org/10.1016/j.jcat.2017.08.025>).